High-efficiency, 80-mm aperture metalens telescope

*Lidan Zhang, †‡ Shengyuan Chang, †‡ Xi Chen, † Yimin Ding, † Md Tarek Rahman, †Yao Duan, † Mark Stephen, ⊥ and Xingjie Ni †**

† Department of Electrical Engineering, the Pennsylvania State University, University Park, PA 16802, United States
⊥ NASA-Goddard Space Flight Center, Greenbelt, MD 20771, United States

KEYWORDS: metalens, telescope, large-scale, metasurface, all-dielectric, DUV lithography

ABSTRACT: Metalenses promise potential for a paradigm shift of conventional optical devices. However, the aperture sizes of metalenses are usually bound within hundreds of micrometers by the commonly-used fabrication methods, limiting their usage on practical optical devices like telescopes. Here, for the first time, we demonstrate a high-efficiency, single-lens, refractive metalens telescope. We developed a mass production-friendly workflow for fabricating wafer-scale (80-mm aperture) metalenses using deep-ultraviolet (DUV) photolithography. Our metalens works in the near-infrared region with nearly diffraction-limited focal spot sizes and a high peak focusing efficiency of 80.84% at 1450 nm experimentally. Based on the metalens, we built a single-lens telescope and acquired images of the lunar surface, revealing its geographical structures. We believe our demonstration of the metalens telescope proves the exciting potential lying in the metasurfaces and could bring new possibilities for areas involving large optical systems, including geosciences, planetary observation, and astrophysical science.

Not long after its first appearance, the telescope found its place in astronomy[1] and became our sail to reach for the stars ever since. To this day, humans have constructed telescopic systems that are both land-based and space-borne, revealing valuable insights into our galaxy and the universe. However, the resolving power of telescopes heavily relies on their aperture size, leading to the extreme weight and footprint that bring challenges to their construction and deployment[2]. Similar problems also occur for conventional optical systems relying on complicated multi-element designs to achieve the desired level of optical performance, where elements made of glasses or other refractive materials are bulky and heavy. Moreover, these elements are often cascaded together for aberration correction, leading to a precipitous increase in the size and weight of the system[2–4]. The solution to these problems may surf with recent advances in nanofabrication techniques and the so-called "metasurfaces" – artificial interfaces that mold light with spatially varying subwavelength nanoantennas, *i.e.*, meta-atoms. Being ultrathin and lightweight, metasurfaces have provided a new approach to recasting optical components into flat devices without performance deterioration. [5–8] In particular, metasurface lenses, a.k.a. metalenses, have attracted tremendous attention in the past decade for their ultra-thin planar configurations, which promise a drastic reduction in optical systems' size and weight. [9–11] In addition, metalenses could realize dispersion engineering from chromatic and angular perspectives, which can be utilized to design optical devices ranging from chromatic-aberration-corrected singlets to dispersion-enhanced metalenses for hyperspectral imaging. [12–16] However, despite the numerous advantages mentioned above, the application of metalenses, or meta-optical devices in general, remains elusive due to their limited aperture sizes.

A major reason for this limit lies in the manufacturing processes of meta-optical devices. Currently, electron-beam (e-beam) lithography and focused ion beam (FIB) are commonly used to

define the subwavelength-scale meta-atoms, thanks to their power to resolve nanometer-scale features with high precision. However, being scanning-based techniques, e-beam lithography and FIB come with slow speed, high expense, and limited scalability, making it challenging to fabricate large-aperture meta-optical devices even for mere prototyping, let alone mass production. [17,18] To date, most of the metalenses reported have only (sub-) millimeter scale apertures. In contrast, conventional lenses with at least centimeter-scale apertures are commonly seen in our daily life, even considered entry-level for applications like telescopic imaging. This also implies that if the metasurface can be made with a large aperture and high efficiency, it will become a game-changer in areas previously considered inaccessible to meta-optics, such as planetary observation and remote sensing and imaging. [19–25]

Over the past years, several attempts have been made to develop cost-effective and scalable fabrication techniques for manufacturing large-aperture metalenses. For example, the nano-imprint method has been used to fabricate gallium nitride metalenses with an aperture size of ~1 cm[26]. Although the nano-imprint technology is mass-production friendly, it suffers from pattern defects, low throughput, and template wear[27]. An alternative method for large-scale metalens fabrication is photolithography, which is known for its superior throughput. Using stepper lithography, metalenses with aperture sizes up to 2 cm have been demonstrated in near-infrared and visible wavelengths[28–30]. However, those metalenses are still way smaller than their conventional counterparts. Motivated by this, we addressed this challenge by developing a wafer-sized high-efficiency metalens to build a telescope, along with a complete fabrication workflow to enable its manufacture in a cost-effective, mass-producible fashion.

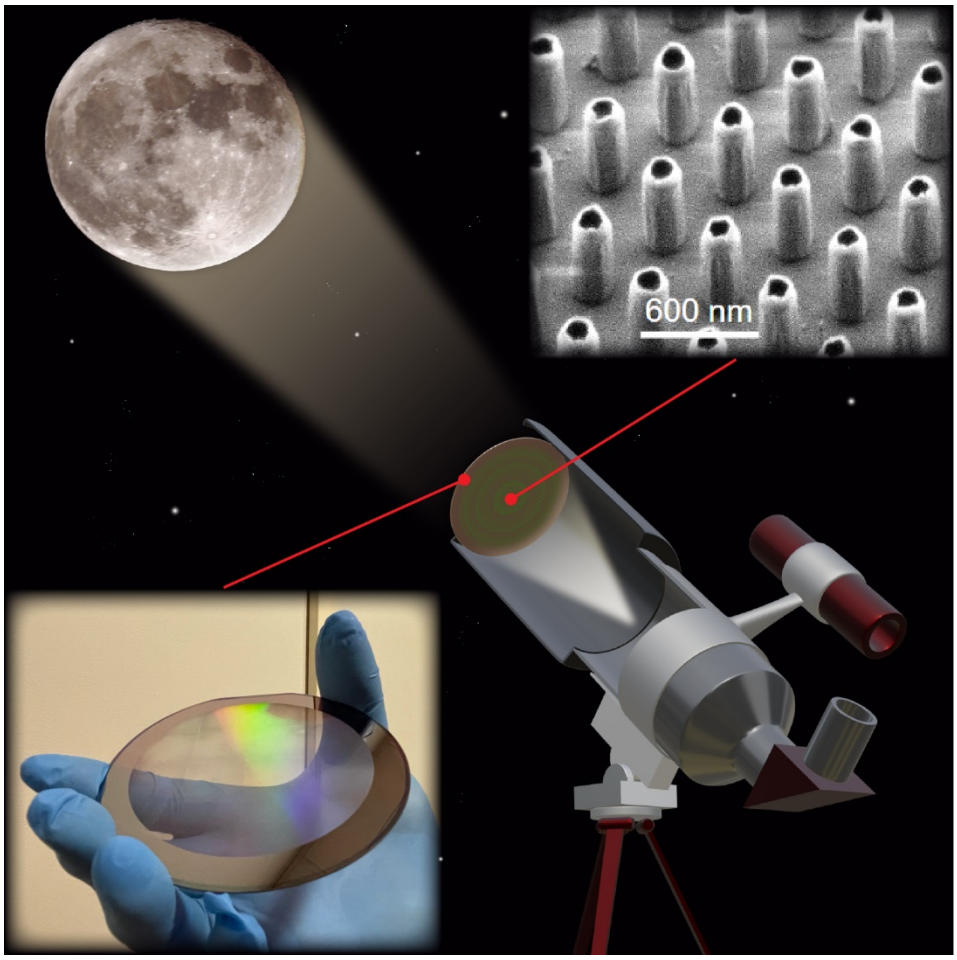

Figure 1. The metalens telescope, with an 80-mm metalens as its objective. A schematic illustration of the metalens telescope. The metalens is used as the telescope objective and focuses light from the moon to form its image. The telescope tube is shown only for illustrative purposes and does not exist in our actual setup. The image capture system, including a camera and a filter, is omitted for simplicity. (Top inset) An SEM image of its constituent meta-atoms, scale bar: 600nm. (Bottom inset) A photograph of the fabricated wafer-scale metalens.

Here, for the first time, we demonstrate an 80-mm aperture, high-efficiency, refractive metalens telescope capable of observing celestial bodies such as the moon (Figure 1). The metalens with an unprecedented 80-mm aperture (bottom left inset, Figure 1), the core part of our telescope, was

first designed numerically and then fabricated on a four-inch silicon wafer with deep-ultraviolet (DUV) projection stepper lithography (top right inset, Figure 1), which is commonly used in the semiconductor industry. Its focusing and imaging performance was tested through a series of experiments conducted both indoors and outdoors. The focusing efficiency of our metalens reached a peak of 80.84%, measured at 1450 nm. Further imaging and video recording tests with either a standard resolution test target or real-life objects demonstrated our metalens' superior resolving power and light collection efficiency. Finally, we built the metalens telescope and acquired images of the moon's surface. To the best of our knowledge, this is the first time the metalens was used for celestial imagery.

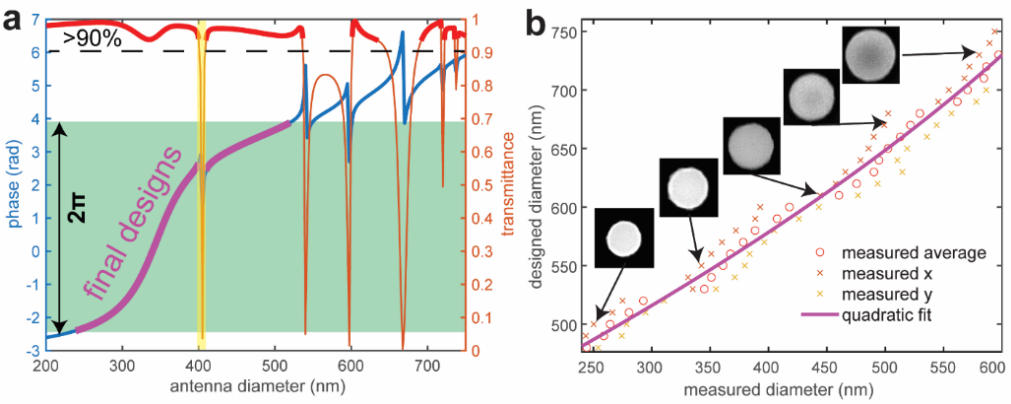

Figure 2. Design principles and size-correction method for the meta-atoms. (a) The simulated phase and transmittance response of amorphous silicon nanocylinders with different diameters ranging from 200 nm to 800 nm. The antennas with diameters ranging from 240 nm to 520 nm were selected as the final designs (purple line inside green shaded area), covering a complete 2π phase range. A resonance regime around 400 nm diameter was excluded due to the low transmittance and rapid phase changes. The transmittance for our designs is over ~95%. (b) fabrication test result for the relationship between the measured diameter of the fabricated

nanocylinders and the designed diameters in the input layout. With the appropriate dose for the exposure, our smallest design (240 nm diameter) can be fabricated with a pattern size of 480 nm, corresponding to 1.9 μm in the reticles (magnified by four times), which the mask writer can achieve. (Insets) SEM images of the fabricated nanocylinders of different sizes.

Our large-aperture metalens, the core of the metalens telescope, was designed by calculating the required phase profile $\varphi(r) = -\frac{2\pi}{\lambda}[\sqrt{(r^2 + f^2)} - f]$, where f is the focal length of the metalens, λ is the wavelength of the incident light, and r is the radial position on the lens. We designed nanocylinder antennas, which are the meta-atoms of our metalenses, made of amorphous silicon on a fused silica substrate. Simulating the nanocylinders using a full-wave solver, we found that a complete 2π phase coverage can be achieved with nanocylinders' diameters ranging from 240 to 520 nm (Figure 2(a)). A resonance near 400 nm is excluded to ensure a smooth change of phase. In addition, only antennas with greater than 95% transmittance were chosen to ensure the high efficiency of the resulting metalenses. A small metalens with a diameter of 40 μm was designed and simulated to validate our meta-atom designs (see Supplementary Note S1).

In order to achieve accurate sizes for our patterns, we first established the relationship between the input meta-atom dimensions and the fabricated meta-atom dimensions measured in scanning electron micrographs (SEMs) by multiple dose- and etching- tests (Figure 2(b)). We then use a quadratic fitting to relate the meta-atom dimensions in the layout and the fabricated patterns, which guarantees that the fabricated antennas' dimensions match the required ones. To reduce the layout file size to a reasonable level, we took advantage of the radial symmetry of the metalens phase profile. We only stored a lookup table (LUT) and the meta-atom positions. The circular cross-sections of the corresponding meta-atoms were approximated with polygons. The designs of the

meta-atoms were determined based on their positions via the LUT. For our 80-mm metalens, the layout file is about 240 GB with a 5-nm increment in meta-atom diameters. Our pattern layout files were generated corresponding to the required phase profile with both correction and compression.

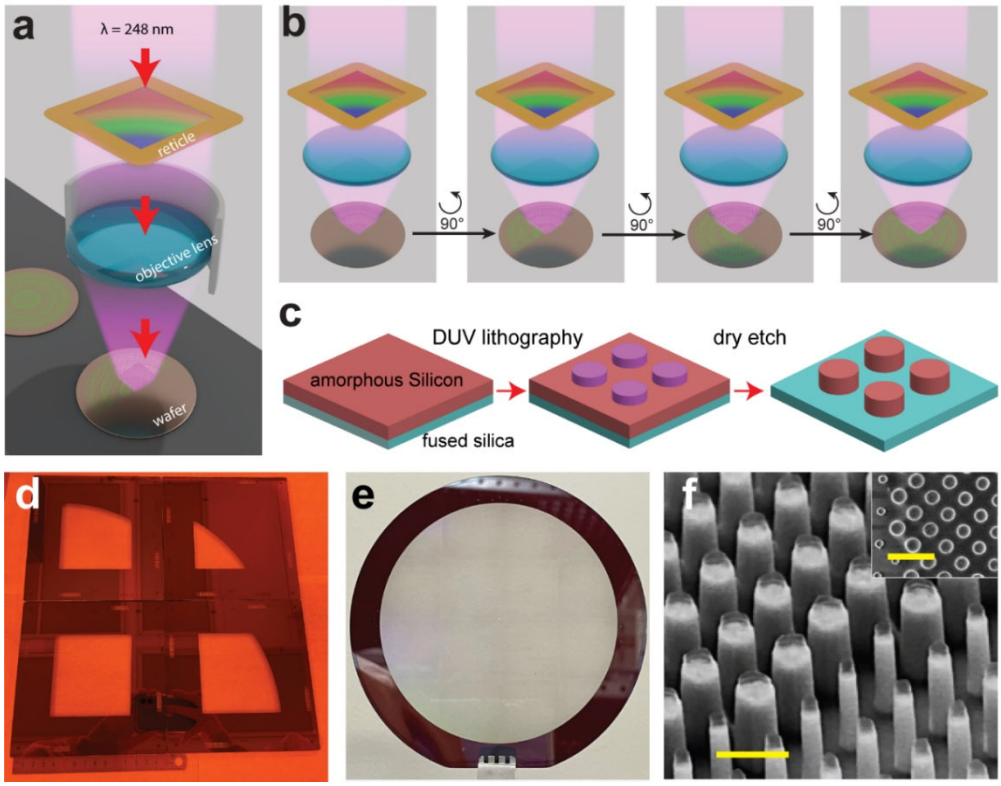

Figure 3. Fabrication results of the wafer-scale metalenses. (a) A schematic illustration of the exposure process of DUV lithography for large-scale metalenses fabrication. A light source with a 248 nm wavelength is used for the DUV stepper system. The patterns on the reticles (photomasks) are projected to the wafer through projection lenses with 4:1 reduction, generating up to a 22-mm-by-22-mm area with a single exposure. (b) The rotating method is used during DUV exposure. By rotating the relative position of the reticle and the wafer with prefabricated rotation markers by 90°, the exposure can be realized in different quadrants of the metalens. Either reticles or wafers can be rotated. But the reticles can only rotate for 90° in the loading process, while the wafers can be rotated for an arbitrary angle using the stage controller, which provides

more flexibility. (c) A schematic of the fabrication process flow. A thin amorphous silicon film was deposited on a fused silica wafer. DUV lithography was followed to make the resist pattern, and then the resist pattern was transferred to amorphous silicon film by dry etching. (See Methods and Supplementary Note S2) (d) A photograph of the four reticles used in the DUV lithography process. (e) A photograph of the final 80-mm-aperture metalens. (f) A tilted-beam scanning electron micrograph (SEM) of metalens reveals nanocylinders of different sizes and vertical sidewalls. (Inset) A top-view SEM of the metalens. The thin residual layer on top of the pillars is a conductive polymer that we used to reduce the charging effect when taking the SEM image. It was removed after the SEM imaging. Scale bars: 1 μm.

We fabricated our metalens with our customized DUV lithography workflow. Considering the maximum area for a single exposure of the DUV tool is a 22-mm-by-22-mm field, we divided our patterns into 16 pieces, with each piece a 20 mm × 20 mm square for exposure. Exploiting the C^4 rotational symmetry of the metalens, only four reticles are needed to cover a quarter of the metalens, simplifying the lithography process. The four reticles were made with the pattern size magnified four times for the projection lithography (Figure 3(a), (d)). Our metalens pattern was transferred onto a four-inch fused silica wafer by a DUV stepper with four reticles at a 4:1 reduction ratio (Figure 3(a)). The exposure process for 16 fields can be done either by reticle rotation (rotation markers needed on the reticles) or wafer rotation (rotation markers needed on wafers) with appropriate stitching for different fields. In the exposure process, four reticles were loaded into the Stepper. A quarter of our metalens pattern, consisting of four 20 mm × 20 mm fields, was exposed through four different reticles. The other three quarters were exposed by rotating the relative position of reticles and wafers by 90°, 180°, and 270° (Figure 3(b)). The

exposed pattern was followed by post-exposure bake and development and then transferred to the amorphous silicon layer below through the inductively coupled plasma reactive ion etching process. The entire process flow is shown in Figure 3(c), and the fabricated metalens is shown in Figure 3(e). We observed that the stitching error among different fields was less than 1 μm (see Supplementary Note S2), which has negligible influence on the performance of the metalens. Characterization of the fabricated metalens by SEM shows that the constituent nanocylinder antennas match well with our design (Figure 3(f) and top left inset of Figure 1). In summary, our DUV photolithography-based fabrication method embraces both precision and simplicity while eliminating the need for scanning-based pattern writing, thus significantly reducing cost and time and being suitable for the mass production of commercial telescopes.

With the metalens fabricated, we characterized the optical performance specifications of the fabricated metalens with a homemade optical platform. For focusing measurements, the point spread function (PSF) was captured using an imaging system, as shown in Figure 4(a) (see Supplementary Note S3). By tuning the output wavelength of the incident light and translating the objective lens along the optical axis, we characterized the intensity profile of the focused beams along both yOz and xOy cross-sections over a broad wavelength range, from 1200 nm to 1600 nm (Figure 4(b)). Our measurement shows that, although the metalens was designed to operate at the 1450 nm wavelength, it could still focus light tightly across the tested wavelength range, with varying focal lengths due to diffractive dispersion. The measured focal lengths show a roughly linear dependence with the incident wavelength (Figure 4(c)). Further, the quality of each focal spot was evaluated by extracting its full width at half maximum (FWHM) and comparing it to that of a diffraction-limited system with the same numerical aperture (NA). The results show that the measured FWHMs were close to diffraction-limited values across all wavelengths (Figure 4(d)).

Note that the NAs used for determining the diffraction-limited spot sizes were calculated based on the metalens aperture size and the measured focal lengths at each wavelength.

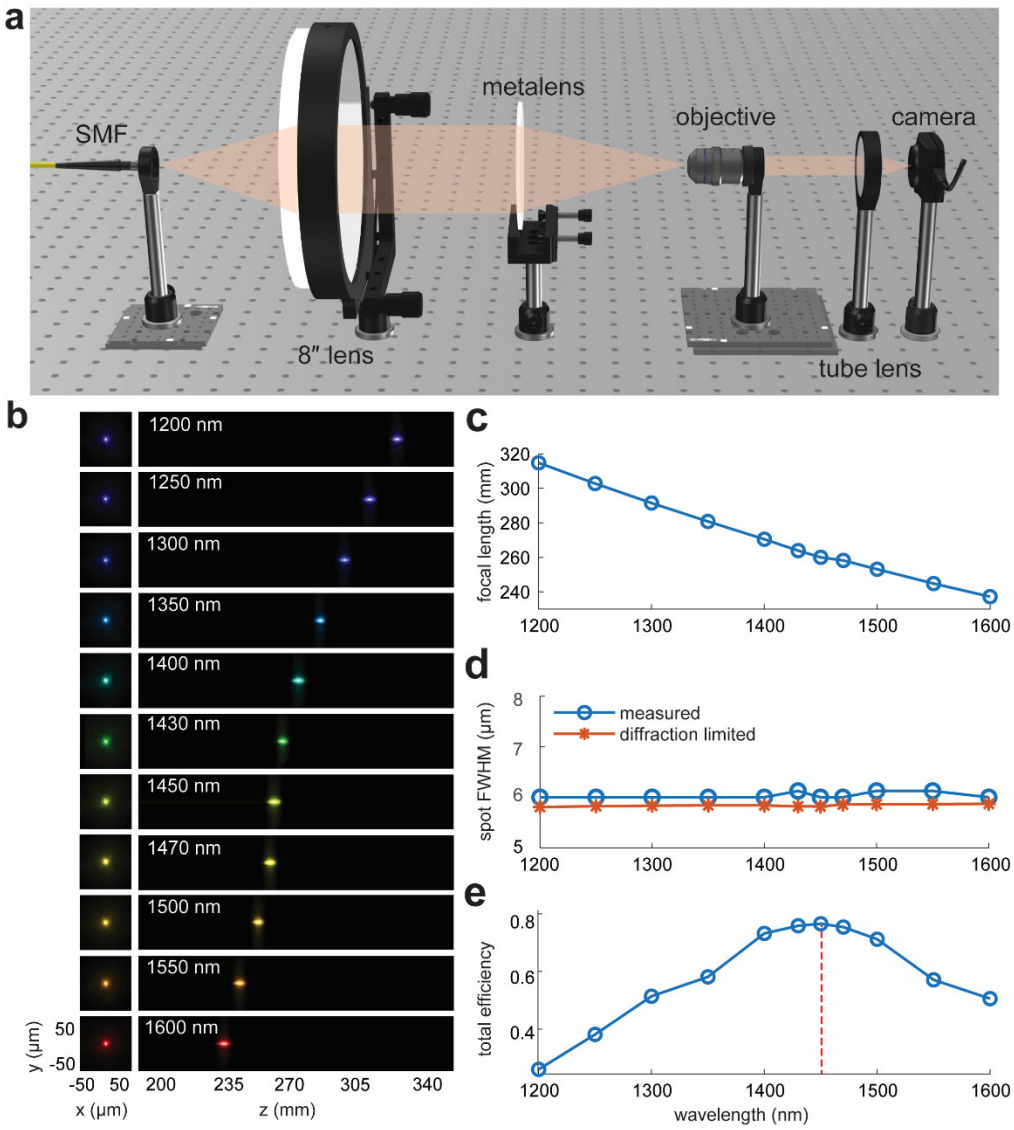

Figure 4. Focusing performance of the fabricated metalens. (a) A schematic of the experimental setup for characterizing the focusing performance of the metalens. The laser out-coupled from a single-mode fiber was expanded and collimated by an 8-inch lens (Edmund Optics PCX Condenser Lens #27-513, effective focal length 400 mm) to ensure the incident beam size is much larger than the metalens aperture. (b) Intensity profiles of the focused beam after the metalens along both xOy

and yOz cross-sections with the wavelength ranging from 1200 nm to 1600 nm. (c-f) Measured focusing properties of the fabricated metalens with the wavelength ranging from 1200nm to 1600nm: (c) The focal lengths, (d) focal spot FWHM and (e) total focusing efficiency.

The Strehl ratio (SR) is a criterion commonly used in optical industries to characterize the aberrations of the optical system. [31] We calculated the Strehl ratio of our metalens imaging system through the measured PSF in the following way. [32] First, we calculated the ideal PSF based on the diffraction-limited FWHM value (FWHM = 0.514 λ/NA) and normalized the ideal PSF so that its value at the center equals unity. Second, we normalized the measured PSF to have the same integral as the ideal PSF across the cross-section. Finally, the ratio of the measured and ideal integral values is the SR. The calculated SR of our metalens system (Figure S4) is around 0.5 for all the wavelengths. However, we would like to note that this SR indicates the focusing performance of the entire measurement system rather than the metalens alone. It was significantly affected by our measurement instruments, for instance, the imperfection of the input wavefront caused by the 8-inch plano-convex collimation lens which has a large spherical aberration. This SR value does not directly represent the actual performance of our metalens. However, after further analysis, we find the SR of the system is around 0.7 even if we replace the metalens with a perfect lens in our measurement system (Supplementary note S5). This indicates that our metalens did perform well, which is not much worse than an ideal lens. The discrepancy mainly originated from other limiting factors such as substrate thickness non-uniformity, fabrication imperfections, etc.

Finally, we measured the focusing efficiencies of our metalenses using an optical power meter. In order to accurately measure the input intensity distribution before the metalens and the focused power, we mounted a pinhole in front of the photodetector. The purpose of the pinhole is twofold:

(1) to sample the intensity distribution in front of the metalens and fit with a two-dimensional Gaussian profile to determine the incident light power; (2) to limit the detector aperture to only capture light within an area across about three times of the FWHM of the focal spot size at the metalens focal plane. Details of the efficiency measurement can be found in the supplementary material. Our measured focusing efficiency reaches its maximum at 1450 nm, with a value of 80.84% (Figure 4(e)). Compared to previously reported works, this efficiency is among the highest values reached by metalenses operating at a single wavelength. These results suggest that, with a tight focus as well as excellent efficiency, our metalens can serve as a telescope objective.

Next, we tested the imaging performance of our metalens in both laboratory and outdoor environments to determine its resolving power. First, we imaged the USAF 1951 resolution test chart with the single-lens imaging configuration and the as-captured grayscale image (Figure 5(a-b)). A beam expander and bandpass filter were used to ensure uniform monochromatic illumination (see Methods section). The smallest feature we could resolve is Group 5, Element 6 in the resolution test chart, with a line width of 8.77 μm (57 line pairs/mm). This value is close to the focal spot FWHM we measured earlier, which means we had reached the limit of the resolving power of our metalens. Second, we used the same configuration to image a burning candle. We captured images (Figure 5(c)) and recorded videos of the candle frame (see Supplementary Movie S1).

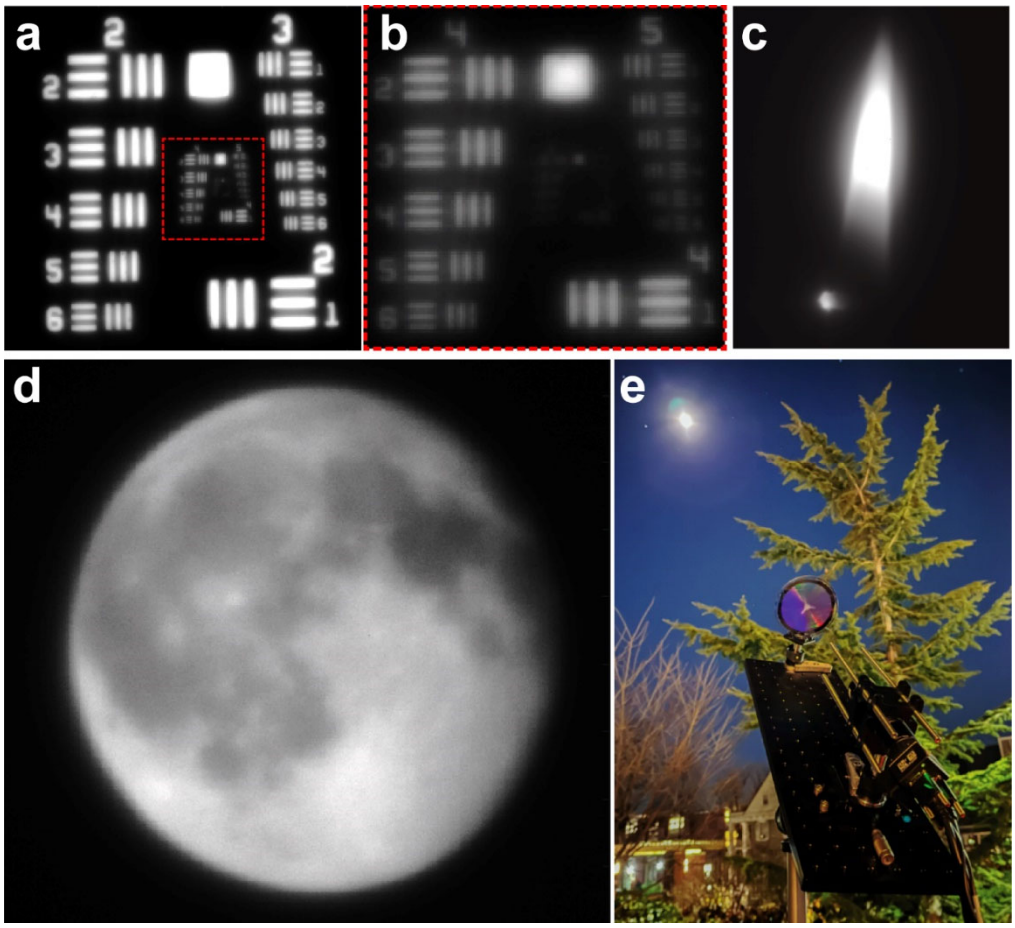

Figure 5. Imaging performance of the fabricated metalens. (a) Captured images of the USAF 1951 resolution chart formed by the 4-inch-aperture metalens. (b) Zoomed-in view of the red boxed area in (a), showing the center area consisting of patterns from Group 4 and above. (c) Infrared image of the flame from a lit candle. (d) An IR image of the moon formed by the metalens. The image was magnified 2x by a 2f-2f relay system (f_1=25mm, f_2=50mm, bi-convex lenses) in front of the camera. (e) A photograph of the metalens telescope which was being used to capture the moon's image. The same bandpass filter was used to reduce the background noise. All images captured by the camera are without any post-processing.

Finally, we built our metalens telescope with the fabricated metalens as the objective. The image was magnified 2x by an image relay system before being captured by the camera to fully utilize its pixels. The system was assembled on an optical breadboard mounted on a commercial camera tripod. Through this metalens telescope, we imaged the lunar surface in an outdoor environment (Figure 5(d-e)). We identified some features of the lunar surface, such as the Sea of Rains, the Sea of Serenity, the Sea of Tranquility, the Ocean of Storms, the Sea of Tranquility, and the Copernicus crater, from the obtained image. Note that the blurry right edge of the moon was attributed to the Waning Gibbous phase of the moon. We could determine that our metalens telescope's resolution is about 80 km on the lunar surface, which is worse than the theoretical diffraction limit. It is mainly due to the chromatic aberration of the metalens. Another reason for imaging blurring is the aberration of the image relay system. In the future, the resolution can be improved by applying a filter with a much narrower bandwidth. Also, it can be enhanced by designing higher NA metalens and optimizing the telescope setup.

In conclusion, we developed a metalens telescope system capable of celestial imagery based on a high-efficiency, 80-mm aperture metalens. In order to fabricate such large metalens, we leveraged the radial symmetry of the pattern and proposed an approach to fabricate high-performance, large-aperture metalenses with reduced expense and time, which involves the rotation-and-stitching of the pattern and multiple-exposure processes with DUV photolithography. The technique allows us to skip the costly, time-consuming scanning-based lithography processes for large-area densely packed nanostructures. The symmetries of the metalens pattern are exploited to significantly reduce the layout file size and the number of reticles needed for photolithography. This developed process can be readily extended for the mass production of large-scale meta-optical components. Through our characterization, we observed that our wafer-scale (80-mm diameter)

metalenses have nearly diffraction-limited focal spot sizes and over 80% peak focusing efficiency at 1450 nm. The metalens underwent a series of imaging tests to determine its resolving power and was used in the metalens telescope to acquire images of the lunar surface.

Metalens is inherently free from spherical aberration, and its ultrathin thickness makes them ideal as an alternative to the bulky lens groups, which are an essential part of modern telescope systems for aberration correction. Although our metalens telescope design is limited to single wavelength imaging in near-infrared, the metalens telescope can be further improved with achromatic designs for better imaging performance. Currently, there is no practical design for achromatic metalens with an aperture size at our scale (several tens of millimeters), but possible schemes are being discussed.[33] Nevertheless, our developed DUV lithography technique can readily fabricate achromatic metalenses once the designs with a manufacturable minimum feature size become available. Besides, the resolution of DUV lithography can be further improved by reducing the feature size in reticle fabrication by an advanced mask writer and carefully controlling the DUV conditions, which allows for extending the working wavelength to visible light.

The demonstrated metalens telescope could be a compact, versatile, and energy-efficient imagery sub-system for remote sensing and imaging systems for aircraft, unmanned vehicles, drones, and satellites, as well as consumer products such as virtual reality (VR), augmented reality (AR), and mixed reality (MR) devices. The developed fabrication technique could lead to highly scalable, cost-effective mass production of large-aperture metalenses and can be readily extended to other large-scale nanostructured patterns. We believe our work could impact the greater metamaterials, electromagnetics, and optical research communities.

Methods

Fabrication. Our metalens is fabricated on a 4-inch fused silica substrate. First, 1 μm of amorphous silicon was grown on top of the substrate by plasma-enhanced chemical vapor deposition (PECVD). Then the anti-reflective coating and photoresist were spin-coated on top of amorphous silicon, followed by pre-baking. Next, the wafer was exposed using a KrF excimer laser of an ASML DUV stepper with four reticles through the rotation and stitching process. We use Heidelberg MaskWriter DWL2000 to write the reticles, and the size is magnified patterns of our layout by four times for ASML stepper usage. (Further details can be found in Supplementary note S2)

Optical characterization. For focusing capability measurements, laser output from a single-mode fiber end was collimated by an 8-inch-aperture plano-convex lens (effective focal length: 400 mm), which expanded the beam diameter to ~100 mm. The focal spot behind the metalens was imaged by an infinity-corrected imaging system. The imaging system has a magnification of 50x. For imaging capability measurements, the USAF resolution test chart was illuminated by a halogen lamp. The light from the lamp was expanded using a 2F-2F relay system with 2x magnification to get a more uniform illumination. A bandpass filter (Thorlabs FB1450-12), with a 1450 nm central wavelength and a 12 nm bandwidth, was mounted on the camera to reduce the background noise. Further details of the focusing and imaging tests can be found in Supplementary Note S3.

ASSOCIATED CONTENT

Supporting Information.

The Supporting Information is available free of charge at XXXXX

1. Meta-atom design and simulation details, fabrication process and error analysis, optical characterization details, and detailed discussion on the metalens Strehl ratio measurement

2. A video clip of a burning candle's frame recorded by the large-scale metalens

AUTHOR INFORMATION

Corresponding Author

*Xingjie Ni - Department of Electrical Engineering, the Pennsylvania State University, University Park, PA 16802, United States

Email: xingjie@psu.edu

ORCID

Lidan Zhang: 0000-0001-9283-0172

Shengyuan Chang: 0000-0002-4245-2991

Xi Chen: 0000-0001-6718-0745

Yimin Ding: 0000-0002-2159-7825

Yao Duan: 0000-0002-2262-1815

Xingjie Ni: 0000-0001-7405-5678

Author Contributions

‡L.Z. and S.C. contributed equally to this work. X.N. and M.S. conceived the project. X.N. supervised the study. X.N. and X.C. performed the design and numerical simulations. L.Z. developed the fabrication process and fabricated the metalenses. S.C. and L.Z. performed the metalens characterizations. S.C. developed the stage control code and analysis code for metalens characterization. Y.Ding and Y.Duan provided technical support for metalens characterization and fabrication. M.R. helped with film deposition and SEM imaging. L.Z., S.C., and X.N. wrote the manuscript, and all authors discussed the results and commented on the manuscript.

Funding Sources

NASA Early Career Faculty Award (80NSSC17K0528), Office of Naval Research (N00014-18-1-2371), and National Science Foundation (NSF) CAREER Award (ECCS-2047446).

Notes

The authors declare no conflicts of interest.

ACKNOWLEDGMENT

This work was partly performed at the Cornell NanoScale Facility (CNF), a member of the National Nanotechnology Coordinated Infrastructure (NNCI) supported by the National Science Foundation (NNCI-2025233), and the Penn State Nanofabrication Facility. The authors would like to thank J. Treichler, G. Bordonaro, M. Skvarla, J. Clark, and J.-S. Park for their generous help in using the CNF. The authors also acknowledge the support from M. Labella, G. Lavallee, and B. Liu in using the Penn State Nanofabrication Facility.

REFERENCES

(1) Loker, A. *Profiles in Colonial History*; Aleck Loker, 2008.
(2) Born, M.; Wolf, E. *Principles of Optics: Electromagnetic Theory of Propagation, Interference and Diffraction of Light*, 7th ed.; Cambridge University Press: Cambridge, 1999. https://doi.org/10.1017/CBO9781139644181.
(3) Stone, T.; George, N. Hybrid Diffractive-Refractive Lenses and Achromats. *Appl. Opt., AO* **1988**, *27* (14), 2960–2971. https://doi.org/10.1364/AO.27.002960.
(4) Buralli, D. A.; Rogers, J. R. Some Fundamental Limitations of Achromatic Holographic Systems. *J. Opt. Soc. Am. A, JOSAA* **1989**, *6* (12), 1863–1868. https://doi.org/10.1364/JOSAA.6.001863.
(5) Chang, S.; Guo, X.; Ni, X. Optical Metasurfaces: Progress and Applications. *Annual Review of Materials Research* **2018**, *48* (1), 279–302. https://doi.org/10.1146/annurev-matsci-070616-124220.
(6) Kamali, S. M.; Arbabi, E.; Arbabi, A.; Faraon, A. A Review of Dielectric Optical Metasurfaces for Wavefront Control. *Nanophotonics* **2018**, *7* (6), 1041–1068. https://doi.org/10.1515/nanoph-2017-0129.
(7) Yu, N.; Capasso, F. Flat Optics with Designer Metasurfaces. *Nature Mater* **2014**, *13* (2), 139–150. https://doi.org/10.1038/nmat3839.
(8) Kildishev, A. V.; Boltasseva, A.; Shalaev, V. M. Planar Photonics with Metasurfaces. *Science* **2013**, *339* (6125), 1232009–1232009. https://doi.org/10.1126/science.1232009.
(9) Chen, W. T.; Zhu, A. Y.; Sanjeev, V.; Khorasaninejad, M.; Shi, Z.; Lee, E.; Capasso, F. A Broadband Achromatic Metalens for Focusing and Imaging in the Visible. *Nature Nanotech* **2018**, *13* (3), 220–226. https://doi.org/10.1038/s41565-017-0034-6.
(10) Wang, S.; Wu, P. C.; Su, V.-C.; Lai, Y.-C.; Chen, M.-K.; Kuo, H. Y.; Chen, B. H.; Chen, Y. H.; Huang, T.-T.; Wang, J.-H.; Lin, R.-M.; Kuan, C.-H.; Li, T.; Wang, Z.; Zhu, S.; Tsai, D. P. A Broadband Achromatic Metalens in the Visible. *Nature Nanotech* **2018**, *13* (3), 227–232. https://doi.org/10.1038/s41565-017-0052-4.
(11) Yu, N.; Genevet, P.; Kats, M. A.; Aieta, F.; Tetienne, J.-P.; Capasso, F.; Gaburro, Z. Light Propagation with Phase Discontinuities: Generalized Laws of Reflection and Refraction. *science* **2011**, *334* (6054), 333–337.
(12) Arbabi, E.; Arbabi, A.; Kamali, S. M.; Horie, Y.; Faraon, A. Controlling the Sign of Chromatic Dispersion in Diffractive Optics with Dielectric Metasurfaces. *Optica, OPTICA* **2017**, *4* (6), 625–632. https://doi.org/10.1364/OPTICA.4.000625.
(13) Chen, W. T.; Zhu, A. Y.; Sisler, J.; Bharwani, Z.; Capasso, F. A Broadband Achromatic Polarization-Insensitive Metalens Consisting of Anisotropic Nanostructures. *Nat Commun* **2019**, *10* (1), 355. https://doi.org/10.1038/s41467-019-08305-y.
(14) Yesilkoy, F.; Arvelo, E. R.; Jahani, Y.; Liu, M.; Tittl, A.; Cevher, V.; Kivshar, Y.; Altug, H. Ultrasensitive Hyperspectral Imaging and Biodetection Enabled by Dielectric Metasurfaces. *Nat. Photonics* **2019**, *13* (6), 390–396. https://doi.org/10.1038/s41566-019-0394-6.
(15) Faraji-Dana, M.; Arbabi, E.; Kwon, H.; Kamali, S. M.; Arbabi, A.; Bartholomew, J. G.; Faraon, A. Hyperspectral Imager with Folded Metasurface Optics. *ACS Photonics* **2019**, *6* (8), 2161–2167. https://doi.org/10.1021/acsphotonics.9b00744.

(16) Chen, M. K.; Wu, Y.; Feng, L.; Fan, Q.; Lu, M.; Xu, T.; Tsai, D. P. Principles, Functions, and Applications of Optical Meta-Lens. *Advanced Optical Materials* **2021**, *9* (4), 2001414. https://doi.org/10.1002/adom.202001414.
(17) Su, V.-C.; Chu, C. H.; Sun, G.; Tsai, D. P. Advances in Optical Metasurfaces: Fabrication and Applications [Invited]. *Opt. Express, OE* **2018**, *26* (10), 13148–13182. https://doi.org/10.1364/OE.26.013148.
(18) Baracu, A. M.; Avram, M. A.; Breazu, C.; Bunea, M.-C.; Socol, M.; Stanculescu, A.; Matei, E.; Thrane, P. C. V.; Dirdal, C. A.; Dinescu, A.; Rasoga, O. Silicon Metalens Fabrication from Electron Beam to UV-Nanoimprint Lithography. *Nanomaterials* **2021**, *11* (9), 2329. https://doi.org/10.3390/nano11092329.
(19) Luo, X.; Zhang, F.; Pu, M.; Guo, Y.; Li, X.; Ma, X. Recent Advances of Wide-Angle Metalenses: Principle, Design, and Applications. *Nanophotonics* **2022**, *11* (1), 1–20. https://doi.org/10.1515/nanoph-2021-0583.
(20) Song, W.; Liang, X.; Li, S.; Li, D.; Paniagua-Domínguez, R.; Lai, K. H.; Lin, Q.; Zheng, Y.; Kuznetsov, A. I. Large-Scale Huygens' Metasurfaces for Holographic 3D Near-Eye Displays. *Laser & Photonics Reviews* **2021**, *15* (9), 2000538. https://doi.org/10.1002/lpor.202000538.
(21) Byrnes, S. J.; Lenef, A.; Aieta, F.; Capasso, F. Designing Large, High-Efficiency, High-Numerical-Aperture, Transmissive Meta-Lenses for Visible Light. *Opt. Express, OE* **2016**, *24* (5), 5110–5124. https://doi.org/10.1364/OE.24.005110.
(22) Zou, X.; Zheng, G.; Yuan, Q.; Zang, W.; Chen, R.; Li, T.; Li, L.; Wang, S.; Wang, Z.; Zhu, S. Imaging Based on Metalenses. *PhotoniX* **2020**, *1* (1), 2. https://doi.org/10.1186/s43074-020-00007-9.
(23) Moon, S.-W.; Kim, Y.; Yoon, G.; Rho, J. Recent Progress on Ultrathin Metalenses for Flat Optics. *iScience* **2020**, *23* (12), 101877. https://doi.org/10.1016/j.isci.2020.101877.
(24) Phan, T.; Sell, D.; Wang, E. W.; Doshay, S.; Edee, K.; Yang, J.; Fan, J. A. High-Efficiency, Large-Area, Topology-Optimized Metasurfaces. *Light Sci Appl* **2019**, *8* (1), 48. https://doi.org/10.1038/s41377-019-0159-5.
(25) Zhao, F.; Zhao, F.; Shen, Z.; Wang, D.; Xu, B.; Chen, X.; Chen, X.; Yang, Y.; Yang, Y. Synthetic Aperture Metalens. *Photon. Res., PRJ* **2021**, *9* (12), 2388–2397. https://doi.org/10.1364/PRJ.440185.
(26) Brière, G.; Ni, P.; Héron, S.; Chenot, S.; Vézian, S.; Brändli, V.; Damilano, B.; Duboz, J.-Y.; Iwanaga, M.; Genevet, P. An Etching-Free Approach Toward Large-Scale Light-Emitting Metasurfaces. *Advanced Optical Materials* **2019**, *7* (14), 1801271. https://doi.org/10.1002/adom.201801271.
(27) Li, N.; Xu, Z.; Dong, Y.; Hu, T.; Zhong, Q.; Fu, Y. H.; Zhu, S.; Singh, N. Large-Area Metasurface on CMOS-Compatible Fabrication Platform: Driving Flat Optics from Lab to Fab. *Nanophotonics* **2020**, *9* (10), 3071–3087. https://doi.org/10.1515/nanoph-2020-0063.
(28) Ni, H.; Yuan, G.; Sun, L.; Chang, N.; Zhang, D.; Chen, R.; Jiang, L.; Chen, H.; Gu, Z.; Zhao, X. Large-Scale High-Numerical-Aperture Super-Oscillatory Lens Fabricated by Direct Laser Writing Lithography. *RSC Advances* **2018**, *8* (36), 20117–20123. https://doi.org/10.1039/C8RA02644K.
(29) Park, J.-S.; Zhang, S.; She, A.; Chen, W. T.; Lin, P.; Yousef, K. M. A.; Cheng, J.-X.; Capasso, F. All-Glass, Large Metalens at Visible Wavelength Using Deep-Ultraviolet Projection Lithography. *Nano Lett.* **2019**, *19* (12), 8673–8682. https://doi.org/10.1021/acs.nanolett.9b03333.

(30) Hu, T.; Zhong, Q.; Li, N.; Dong, Y.; Xu, Z.; Fu, Y. H.; Li, D.; Bliznetsov, V.; Zhou, Y.; Lai, K. H.; Lin, Q.; Zhu, S.; Singh, N. CMOS-Compatible a-Si Metalenses on a 12-Inch Glass Wafer for Fingerprint Imaging. *Nanophotonics* **2020**, *9* (4), 823–830. https://doi.org/10.1515/nanoph-2019-0470.
(31) Mahajan, V. N. *Optical Imaging and Aberrations*; SPIE: 1000 20th Street, Bellingham, WA 98227-0010 USA, 2001. https://doi.org/10.1117/3.415727.
(32) Khorasaninejad, M.; Zhu, A. Y.; Roques-Carmes, C.; Chen, W. T.; Oh, J.; Mishra, I.; Devlin, R. C.; Capasso, F. Polarization-Insensitive Metalenses at Visible Wavelengths. *Nano Lett.* **2016**, *16* (11), 7229–7234. https://doi.org/10.1021/acs.nanolett.6b03626.
(33) Li, Z.; Lin, P.; Huang, Y.-W.; Park, J.-S.; Chen, W. T.; Shi, Z.; Qiu, C.-W.; Cheng, J.-X.; Capasso, F. Meta-Optics Achieves RGB-Achromatic Focusing for Virtual Reality. *Science Advances* **2021**, *7* (5), eabe4458. https://doi.org/10.1126/sciadv.abe4458.